Research Article Vol. 33, No. 4 / 24 Feb 2025 / Optics Express 7081
Optics EXPRESS

Trap-loss fluorescence spectroscopy of cesium magneto-optical trap with single-photon Rydberg excitation and the background electric field measurement and regulation

XIAOKAI HOU,[1] YUEWEI WANG,[1] WENJING SU,[1] JUN HE,[1,2] AND JUNMIN WANG[1,2,*]

[1]State Key Laboratory of Quantum Optics Technologies and Devices, and Institute of Opto-Electronics, Shanxi University, Tai Yuan 030006, Shanxi Province, China
[2]Collaborative Innovation Center of Extreme Optics, Shanxi University, Tai Yuan 030006, Shanxi Province, China
*wwjjmm@sxu.edu.cn

Abstract: Calibration and compensation of the background electric fields in the vicinity of the cold atomic ensemble are critically vital, for achieving quantum computing, quantum simulation, and precision measurement. Here the work presents and demonstrates a straightforward method for measuring and compensation of the background electric field by means of the trap-loss fluorescence spectroscopy (TLFS) of cesium (Cs) magneto-optical trap (MOT) with the Rydberg $nP_{3/2}$ states with principal quantum numbers n from 71 to 85. In our experiment, TLFS is induced by single-photon Rydberg excitation with a Cs MOT, utilizing a 319 nm ultraviolet (UV) laser characterized by narrow linewidth (less than 6 kHz), continuous fine-tuning of 1 GHZ, and ultra-low-intensity noise (the intensity fluctuates approximately ±0.06% over 25 minutes with sampling power of 3 mW). Using this method, we measure the intensity of the background electric field in the vicinity of a cold atomic ensemble of about 218.9 ± 7.5 mV/cm. Through adjustment of electrode plates the residual electric field was reduced to 116.3 mV/cm, which induces a Stark shift −84.1 MHz. Our experiments provide an easier and more straightforward method for measuring and regulating the background electric field and lay a foundation for optimizing electric field compensation and fast feedback systems in the future.

1. Introduction

Rydberg atoms [1] are a class of atoms characterized by their valence electron being excited to a high principal quantum number, while the atom remains electrically neutral. The distinctive structure of the Rydberg atom, with its valence electrons positioned far from the nucleus, gives rise to its remarkable properties, such as high polarizability, low field ionization threshold, and long-range interactions. Consequently, Rydberg atoms represent a highly promising platform for many-body physics [2], quantum information and computing [3,4], nonlinear optics [5] and imaging [6,7], precision measurement [8–13], among other applications.

In quantum simulation and computing experiments, background electric fields can significantly interfere with the precision of measurements. These background fields, which are often caused by external instrumentation or by ionization processes within the system, lead to errors in the measurement of Stark shifts and thus reduce the accuracy of electric field measurement. To address this challenge, atom-based electric field sensors are developed that offer significant advantages over other methodologies in terms of resolution, sensitivity, and reproducibility. However, the traditional method for detecting the Rydberg state is accomplished via field ionization [14–18], which entails a complex setup and results in the irreversible destruction of the detected atom. Consequently, trap-loss fluorescence spectroscopy (TLFS) based on pure

#549412 https://doi.org/10.1364/OE.549412
Journal © 2025 Received 19 Nov 2024; revised 28 Jan 2025; accepted 30 Jan 2025; published 11 Feb 2025

Optics EXPRESS

optical detection [19–22] has been developed, providing a non-destructive detection method with a simple and user-friendly setup.

In the preparation of cold Rydberg atoms, the Rydberg state is typically detected using cascaded two-photon electromagnetically induced transparency (EIT) [23–25], which is technically simpler to implement and avoids the ultraviolet(UV) band. However, this method suffers from rapid decoherence due to the population of the intermediate state and low excitation rates resulting from significant detuning. Additionally, the multi-photon excitation scheme requires multiple lasers, and the relative phase instability between these lasers contributes to rapid decoherence. Consequently, the preparation of Rydberg atoms via a single-photon excitation scheme [11,12,26–31] can circumvent these issues but necessitates a tunable UV laser system with narrow linewidth. With the rapid advancements in efficient laser frequency conversion technology, UV laser systems have been successfully implemented [11,29], facilitating numerous experiments involving single-photon Rydberg excitation and atomic inner state manipulation [11,32].

In this paper, we present and demonstrate a straightforward method for measuring and evaluating compensation of the background electric field based on TLFS which is induced by single-photon Rydberg excitation utilizing a 319 nm UV laser system within a cesium (Cs) magneto-optical trap (MOT). In Part II, theoretical calculations and analyses of Stark effect are introduced. In Part III, a 319 nm UV laser system is presented as well as cold atoms is trapped in Cs MOT. Subsequently, the TLFS is obtained by single-step Rydberg excitation of cold atomic ensemble trapped in Cs MOT with principal quantum numbers n of 71, 75, 80, and 85, and the intensity of the background electric field in the vicinity of cold atomic ensemble is calibrated by measuring Stark shift between the actual resonant excitation frequency (AREF) and the theoretical excitation frequency of the TLFS at each principal quantum number (derived from the energy level shift due to the DC Stark effect generated by the background electric field), which was approximately 218.9 ± 7.5 mV/cm. Finally, the background electric field is partially compensated by a pair of parallel electrode plates positioned outside the ultra-high vacuum (UHV) glass cell and by changing the angle between the parallel electrode plates and the cell, the residual background electric field intensity is 116.3 mV/cm, and the corresponding Stark shift is −84.1 MHz. The precision compensation of background electric fields is also crucial for achieving reliable and accurate electric field measurements, especially in quantum computing and simulation, where small perturbations can drastically affect system performance.

2. Theoretical analysis and simulations

We first need to simulate and calculate through the theory, as shown in Eq. (1)-(4) [33],

$$\alpha_0 = \frac{2}{3(2J+1)} \sum_{n',l',J'} \frac{\langle n',s',l',J'\|D\|n,s,l,J\rangle^2}{E_{n',l',J'} - E_{n,l,J}} \tag{1}$$

$$\alpha_2 = \sqrt{\frac{40}{3(J+1)(2J+1)(2J+3)}} \times \sum_{n',l',J'} (-1)^{J+J'} \times \begin{Bmatrix} J & 1 & J' \\ 1 & J & 2 \end{Bmatrix} \times \frac{\langle n',s',l',J'\| D \|n,s,l,J\rangle^2}{E_{n',l',J'} - E_{n,l,J}} \tag{2}$$

$$\alpha = \alpha_{core} + \alpha_0 + \alpha_2 \frac{3m_J^2 - J(J+1)}{J(2J-1)} \tag{3}$$

$$\Delta\varepsilon = -\frac{1}{2}\alpha|E|^2 \tag{4}$$

where α_0 is the scalar polarizability, α_2 is the tensor polarizability. α_{core} is the core polarizability of cesium atom, whose value is 15.81 a_0^3 (a_0 is Bohr radius). α is the total atomic polarizability, D

Optics EXPRESS

is the electric dipole transition operator, $\langle n', s', l', J'| \|D\| n, s, l, J\rangle$ is an electric dipole transition matrix element, E is the electric field intensity, $\{\cdots\}$ is the Wigner-6j coefficient and $\Delta\varepsilon$ is the DC Stark shift. Since the vector polarizability α_1 includes the polarization of the laser, it is generally only considered when calculating the AC Stark effect. Therefore, α_0, α_2, and α_{core} need to be considered when calculating and simulating the DC Stark effect produced by the DC electric field. The scalar polarizability, tensor polarizability and total polarizability of the principal quantum number n = 71,75,80 and 85 of the Rydberg state of the Cs atom have been calculated and shown in Table 1.

Table 1. The value of scalar polarizability (α_0), tensor polarizability (α_2) and total polarizability (α) at different principal quantum number and different magnetic quantum number. The unit of polarizability is MHz(V/cm)$^{-2}$

Energy level $\|n, l, J, m_J\rangle$	Scalar polarizability (α_0)	Tensor polarizability (α_2)	Total polarizability (α)
$71P_{3/2}$ m_J=±3/2	16883.4	-1469.3	15414.1
$71P_{3/2}$ m_J=±1/2	16883.4	-1469.3	18352.7
$75P_{3/2}$ m_J=±3/2	25208.9	-2191.4	23017.5
$75P_{3/2}$ m_J=±1/2	25208.9	-2191.4	27400.3
$80P_{3/2}$ m_J=±3/2	40492.3	-3519.8	36972.5
$80P_{3/2}$ m_J=±1/2	40492.3	-3519.8	44012.1
$85P_{3/2}$ m_J=±3/2	63370.1	-5543.7	57826.9
$85P_{3/2}$ m_J=±1/2	63370.1	-5543.7	68913.8

The simulation results are shown in Fig. 1, we chose the Cs Rydberg states $nP_{3/2}$ with principal quantum numbers n = 71, 75, 80, 85 for the measuring. And the DC Stark shifts of each Rydberg state show a negative increasing trend while gradually increasing the DC electric field intensity, i.e., each Rydberg state energy level is red-shifted under the action of the external electric field. Where the dashed and solid lines correspond to two types of Zeeman states of the Rydberg state, (m_J=±3/2) and (m_J=±1/2), respectively. This theoretical simulation is an important tool for our subsequent measurement of the background electric field in the vicinity of cold atomic ensemble as well as for the realization of DC electric field sensing.

In order to verify whether the energy level crossing between the target Rydberg state $nP_{3/2}$ (n=71, 75, 80, and 85) and the adjacent Rydberg state under the action of external DC electric field, we employ the atom calculator [34] to find the Rydberg states close to $nP_{3/2}$ to be (n-1)$D_{3/2}$, (n-1)$D_{5/2}$ and $nP_{1/2}$, respectively. Then, based on Eq. (1)-(4) [33], the energy level shifts of the above Rydberg states under the external DC electric field are calculated separately, as shown in Fig. 2.

In the range of external DC electric field intensitys we are interested in, the Stark shifts of (n-1)$D_{3/2}$ and (n-1)$D_{5/2}$ are positive, i.e., they do not cross with $nP_{3/2}$. However, the Stark shifts of $nP_{1/2}$, which is close to the $nP_{3/2}$, is also negative, and there is an energy level crossing with $nP_{3/2}$ (m_J=±1/2), and the intensity of the external electric field at the crossing decreases with the increase of the principal quantum number n.

The energy level crossing between the target Rydberg state and the adjacent Rydberg state will affect our subsequent background electric field measurements and compensation evaluations. Therefore, based on this phenomenon, we chose to use the Zeeman state of $nP_{3/2}$ (m_J=±3/2) and the Stark shift method to measure the background electric field intensity.

Optics EXPRESS

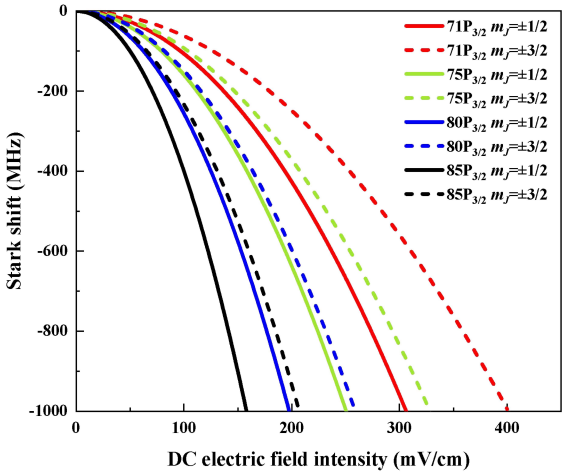

Fig. 1. According to Eq. (1-4), the DC Stark shifts generated within different Zeeman states of $nP_{3/2}$ Rydberg states at different principal quantum numbers n=71, 75, 80 and 85 are calculated while electric field intensity is gradually increasing. Among them, red, green, blue and black represent the principal quantum numbers n = 71, 75, 80 and 85, respectively; The solid line and the dotted line represents m_J=± 1/2 and m_J=± 3/2, respectively.

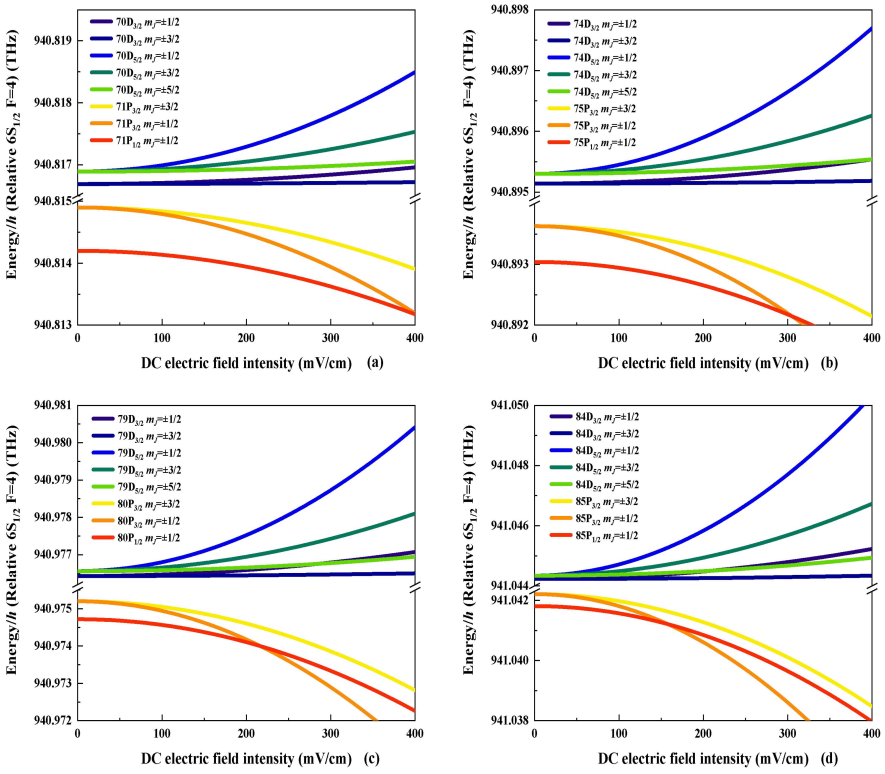

Fig. 2. The energy level map of the Rydberg state in an external DC electric field. According to Eq. (1-4) and the atom calculator, we analyze and simulate the energy level shifts and the crossing generated by an external DC electric field for the four target Rydberg states $nP_{3/2}$ (principal quantum number n is 71, 75, 80 and 85) and the nearest (n-1)$D_{3/2}$, (n-1)$D_{5/2}$ and $nS_{1/2}$ Rydberg states.(a) n=71; (b) n=75; (c) n=80; (d) n=85.

Optics EXPRESS

3. Experimental system

3.1. Preparation of the 319-nm UV laser

Our 319-nm UV laser system for single-step Rydberg excitation of Cs atoms has been developed by ourselves [30,31]. As shown in Fig. 3, we choose 1560 nm distributed feedback Erbium-doped fiber laser (DFB-EDFL) and 1077 nm distributed feedback Ytterbium-doped fiber laser (DFB-YDFL) as the two fundamental-frequency lasers, both of them are amplified by using Erbium-doped fiber amplifier (EDFA) and Ytterbium-doped fiber amplifier (YDFA). Then, combine the beams and pass through MgO-doped periodically poled lithium niobate (PPMgO:LN) crystal to generate 638 nm laser via sum-frequency generation (SFG) process. It is frequency-doubled through a bow-tie-type four-mirror ring cavity with a β-BaB_2O_4 (BBO) crystal inside to obtain 318.6 nm UV laser. Subsequently, we realize the frequency locking of 1560 nm and 638 nm lasers with reference to the ultra-stable cavity by Pound-Drever-Hall (PDH) and Electronics Sidebands (ESB) techniques, respectively, and then achieve the frequency locking and tuning of 319-nm UV laser.

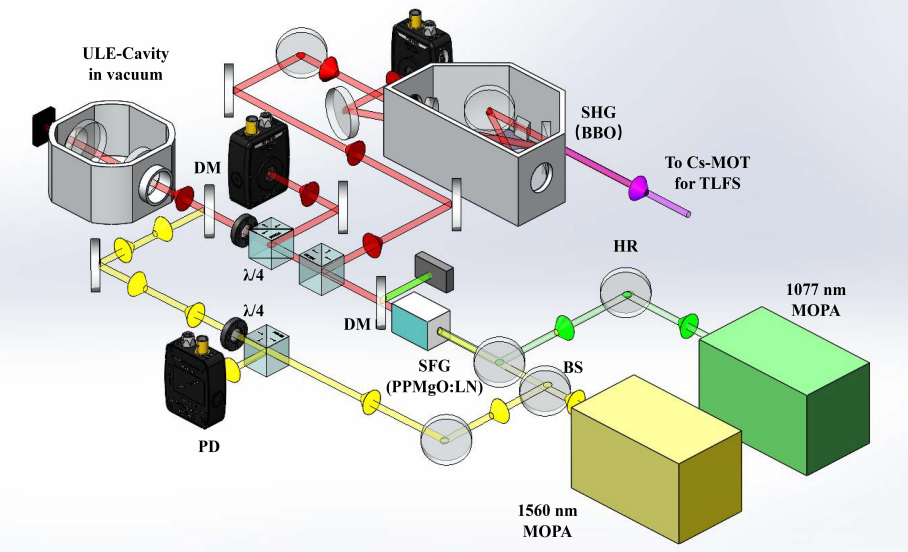

Fig. 3. Apparatus diagram of a 319-nm UV laser system.MOPA, master oscillator power amplifier; BS, beam splitter plate; $\lambda/4$, quarter-wave plates; PBS, polarization beam splitter cube; HR, high reflectivity mirror; DM, dichroic mirror; ULE-Cavity, ultra-low expansion F-P cavity; SFG, sum frequency generation; SHG, second-harmonic generation; PD, photodetector.

3.2. Cs MOT and single-step Rydberg excitation

As illustrated in Fig. 4, the Cs MOT is housed within a $30 \times 30 \times 120$ mm^3 ultra-high vacuum (UHV) glass cell, with typical pressure of approximately 1×10^{-9} Torr. The frequency of the cooling beam, which has a Gaussian diameter of approximately 10 mm, is locked to the Cs $6S_{1/2}$ (F=4) $\rightarrow$ $6P_{3/2}$ (F$'$=5) cycling transition with a detuning of -15 MHz. The repumping beam, with a Gaussian diameter of around 9 mm, is resonant with the Cs $6S_{1/2}$ (F=3) $\rightarrow$ $6P_{3/2}$ (F$'$=4) transition. The cooling and repumping beams are combined and then are divided into three parts: one part along the Z and -Z directions, accounting for approximately 28% of the power. The remaining two parts are split equally in power and directed in the XZ plane at an angle of about 30°. A gradient magnetic field is produced by a pair of anti-Helmholtz coils driven by a constant-current source, generating a typical axial magnetic field gradient of 10 Gauss/cm with

Optics EXPRESS

a current of 1.6 A. Consequently, a bright cloud of cold atomic ensemble can be immediately observed using a CCD camera.

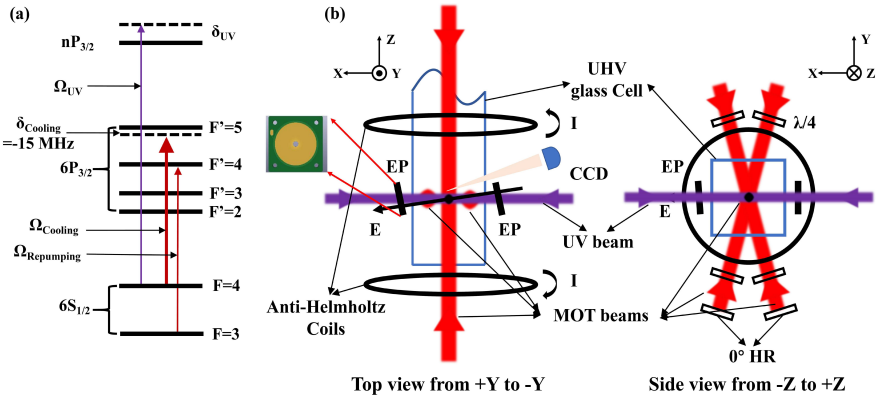

Fig. 4. (a) Diagram of relevant Cs energy level; (b) Schematic diagram of the experimental setup of Cs MOT and the background electric field measurement. The left is top view and the right is side view.

The steady-state clouds of cold atoms in Cs MOT is taken photo using fluorescence imaging at a axial gradient magnetic field of 10 Gauss/cm, with sizes ($1/e^2$ diameter) in the Y and Z directions of 403 μm and 350 μm, respectively. The number of cold atoms is approximately 4×10^6, with an atomic number density of around 2×10^{10} cm^{-3}. We used the simplify time-of-flight (TOF) fluorescence imaging method to measure the effective temperature of cold atoms cloud in the Y and Z directions which are approximately 105.3 ± 3.1 μK and 113.5 ± 2.4 μK, respectively [19].

Based on the above MOT, we employ a 319 nm UV laser for single-step Rydberg excitation targeting the nP$_{3/2}$ state (n=70-85). To prevent the loss of non-Rydberg excited cold atoms in the MOT due to radiation pressure imbalance, we utilize a 319 nm standing wave laser field along the X and -X directions. The laser beams are nearly parallel and have diameters (~ 500 μm) larger than the size of the cold cloud, to cover all cold atoms by the UV laser beam.

4. Trap-loss fluorescence spectroscopy of Cs MOT and Stark shift

4.1. Measurement of background electric field

Since a MOT cannot trap Rydberg atoms, Rydberg atoms are lost when the UV laser couples Cs atoms from the 6S$_{1/2}$ (F=4) to the nP$_{3/2}$ state, achieving single-step Rydberg excitation. In other words, the excitation of Rydberg atoms can be inferred by observing the TLFS from a cold cloud in the MOT.

As shown in Fig. 5(a) and 5(b), the change in frequency of our UV laser system is achieved by scanning it point by point. Each frequency point lasts for 30 s. The CCD camera is triggered for taking the photograph of the cold atom within 30 s, the timestamp of the initial trigger is synchronized, which occurs 5 s after the UV laser is adjusted to the target frequency, and taking the photograph ends at the next time the UV laser frequency is modified, the exposure time of the CCD camera is 5 ms, and the CCD's trigger frequency is 0.2 Hz. In a spectrum acquisition process, each frequency point lasts for 30 s, and the UV laser frequency needs to be changed about 45~55 times, covering about 175~200 MHz, with a total duration of about 30 minutes.

Since the UV Rabi frequency is the order of several hundred kHz, the Rydberg excitation time is must less than the CCD exposure time. Therefore, we believe that the loss of atomic number in the MOT is completely at a steady state within the 5 ms time window. Within 30 s, five fluorescence images of cold atoms will be obtained, and three of them will be randomly

Optics EXPRESS

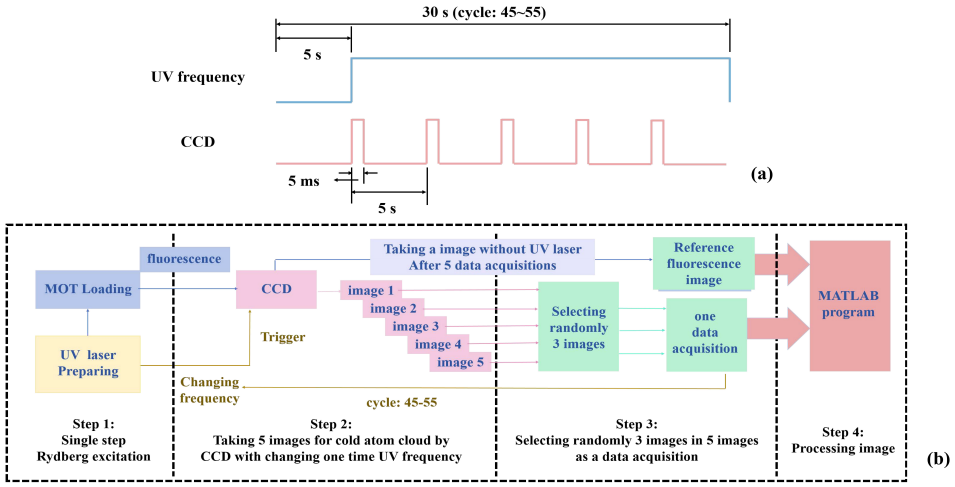

Fig. 5. (a) Diagram of the experimental sequence; (b) Experimental flowchart

selected to calibrate the remaining proportion of cold atoms in the MOT at the current UV laser frequency. For every five data acquisitions, we will take pictures of the MOT that are not Rydberg excited by UV laser for image processing and fluorescence intensity normalization for these five data acquisitions. After a spectral data acquisition, we use a MATLAB program to process the fluorescence images of cold atoms, and the relative fluorescence intensity is calculated by dividing the total fluorescence intensity of the cold atoms in the MOT with UV laser excitation by the reference fluorescence intensity without UV laser excitation. In addition, background light was subtracted to correct for the effect of background scattered light.

Throughout the experiment, we utilize a wavelength meter (HighFinesse, WS-7) to monitor the red light frequency in real time, ensuring the accuracy of the UV frequency. Additionally, the wave meter is calibrated after every five acquisitions using the probe beam ($6S_{1/2}$ (F=4) $\rightarrow$ $6P_{3/2}$ ($F^{'}$=5), 351.72196 THz [35]) as the frequency reference.

In the experiment, the frequency of the cooling laser is fixed to Cs $6S_{1/2}$ (F=4) $\rightarrow$ $6P_{3/2}$ ($F^{'}$=5) cycling transition with detuning of -15 MHz. We chose four different principal quantum numbers Rydberg states (n=71, 75, 80, and 85) as probes to measure the background electric field intensity. when the target Rydberg state is $71P_{3/2}$, the incident power of the UV light is about 20 mW, and the corresponding Rabi frequency is $2\pi\times157$ kHz. And, we reduce the Rabi frequency of the cooling laser until there is no clear AT splitting, in which case the Rabi frequency of the cooling laser is $2\pi\times4.3$ MHz [19,22].

4.2. Regulation and compensation evaluation of background electric field

In our MOT system, some unavoidable problems arise due to the presence of the background electric field. First of all, due to the presence of the frequency shift of the Rydberg state level, the determination of the resonance frequency of the UV laser is a challenge. Secondly, the background electric field in the environment, especially the DC electric field of unknown intensity, will seriously affect the fine control of the strong interaction between Rydberg atoms. Thirdly, we can measure the weak DC electric field on delicate electronic devices by meas of Rydberg atom in the future.

Therefore, the background electric field present in our system must be compensated. We propose a scheme for background electric field regulation and compensation. As shown in Fig. 4(b), a pair of parallel printed circuit board (PCB) electrode plates whose diameter is 25 mm

Optics EXPRESS

are placed on both sides of the UHV glass cell with and a ϕ 4.0-mm hole in the center of plate for optical path. The background electric field is regulated by applying a DC voltage between the PCB electrode plates to artificially change the intensity.

5. Results and discussion

Rydberg atoms have very large electric polarizability and are very sensitive to external electric fields. We can measure the background electric field with the help of this exaggerated property of Rydberg atoms. The background electric field is the comprehensive result of the electric field generated by the instruments and equipments in the external environment, as well as the electric field generated by the ionization of Rydberg atoms. The presence of this background electric field leads to a frequency shift of the Rydberg states of the atoms, which has some effect on the excitation-frequency determination of the UV laser and produces serious errors in our subsequent experiment of DC electric field sensing based on Rydberg atoms.

As shown in Fig. 6, we select the principal quantum numbers of the Rydberg states as n=71, 75, 80, and 85, and obtain the corresponding TLFS under the above parameters,and Lorentzian profile fitting curve where the energy level is $n\mathrm{P}_{3/2}$ ($m_J = \pm 3/2$). Theoretically, the $n\mathrm{P}_{3/2}$ state is composed of four Zeeman states, ($m_J = \pm 1/2$) and ($m_J = \pm 3/2$), and under the action of the electric field, there will be two pits in the TLFS, corresponding to ($m_J = \pm 1/2$) and ($m_J = \pm 3/2$), respectively. In the specific experimental process, the signal-to-noise ratio and reproducibility of the signal corresponding to ($m_J = \pm 1/2$) are poor, so only the results corresponding to ($m_J = \pm 3/2$) are retained.

However, to our surprise, the full width at half maximum (FWHM) of the TLFS measured at four different principal quantum numbers was all on the order of 20 MHz. We propose five possible mechanisms for the linewidth broadening of the TLFS:

Firstly, the Rabi frequency of the cooling laser is still at a relatively high order of magnitude, which still causes the ground state is broadened by a factor of 1.7 due to power broadening. Secondly, The Zeeman broadening in the z-direction at the center of the MOT can be calculated according to $\Delta\Gamma = \frac{\mu_B}{h} g_J(S_{1/2}) \frac{\partial B}{\partial z} \Delta z$. The ground state $6\mathrm{S}_{1/2}$ broadens to 0.96 MHz due to the presence of a magnetic field. Thirdly, our atoms are exposed to severe blackbody radiation (BBR) at room temperature that will directly couple the target Rydberg state with the adjacent Rydberg state.So, the lifetime of the target Rydberg state decreases dramatically, and the typical Rydberg state lifetime is about 10 μs, and the width of the Rydberg state energy level is broadened to 100 kHz. Fourth, as can be seen in Fig. 6, the baseline is less than 100% at the UV laser separation resonance position, there is still a 15% $\sim$ 20% loss of cold atomic fluorescence intensity. This is due to the fact that the cold atoms in the magneto-optical trap are constantly affected by ionization, and we speculate that the mechanisms that lead to ionization are photoionization, field ionization, and collision ionization. Due to the presence of ionization, the overall spectral signal increases by 15% $\sim$ 20%, then we can simply infer that the spectral linewidth is broadened by at least 15% due to the presence of ionization. Last, due to the existence of the ionization mechanism, a cold plasma is formed near the cold atoms, which in turn generates a local electric field of a certain intensity, whose electric field intensity is space-dependent. When such a local electric field is superimposed with the background DC electric field, the Stark shift formed on the Rydberg state will be spatially dependent. It can be roughly inferred that the remaining broadening of about 5 MHz comes from the local electric field generated by the cold plasma [36].

In order to reduce the ionization, we propose two protocol. First, we should avoid the continuous operation of MOT and continuous irradiation of UV laser; second, we believe that it is possible to attenuate the Rabi frequency of UV laser so that the excitation rate is lower than 1/1000 or even lower, forming a unique cat state such as the Rydberg weak dressing ground state. However, this method cannot be characterized by changes in the fluorescence intensity of cold

Optics EXPRESS

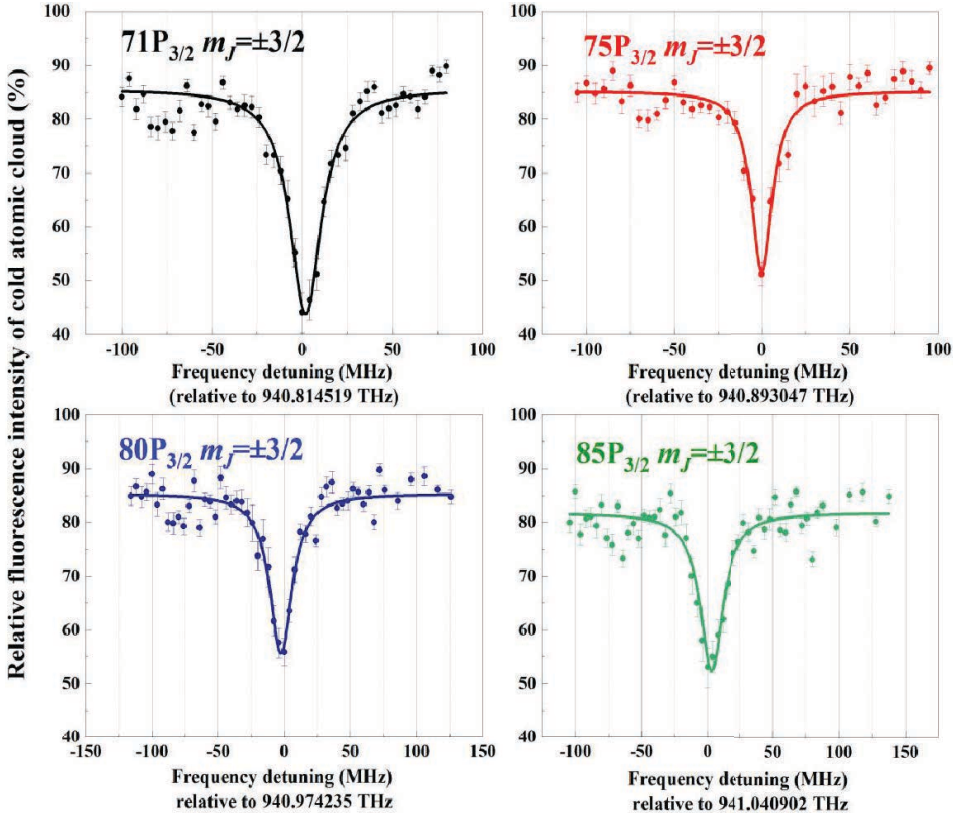

Fig. 6. TLFS at different principal quantum numbers with same rabi frequency of cooling laser of $2\pi\times4.3$ MHz and UV laser of $2\pi\times157$ kHz (a), n=71 (black), (b), n=75 (red), (c), n=80 (blue), and (d), n=85 (green) corresponding to TLFS. The x-axis is frequency detuning of UV laser [realtive to 940.814519 THz (n=71), 940.893047 THz (n=75), 940.974235 THz (n=80), 941.040902 THz (n=85)].

atoms due to the small proportion of Rydberg states. We will measure the external electric field by Ramsay interferometry.

The background eletric field intensity can be measured by measuring the Stark shift. The DC Stark shift due to the background electric field is measured by measuring the difference between the actual resonant excitation frequency (AREF) and the theoretical value [34], and the background electric field intensity corresponding to each principal quantum number Rydberg state is further calibrated according to the simulation results and frequency shift in Fig. 1. We obtained five sets of TLFS at different principal quantum numbers (n=71, 75, 80 and 85), and used the Lorentzian profile to fit them to obtain the AREF of the spectroscopy. The data were then statistically analyzed to obtain the mean and standard deviation of the AREF and listed them in column 2 of Table 2. The third column is the theoretical calculated value of the excitation frequency, and the error should be in the order of Hz, so it is negligible.

By making the difference between the AREF and the theoretical calculated value, the corresponding Stark shift under different principal quantum numbers can be obtained, and the error of the AREF will be linearly transmitted to the Stark shift, which is the fourth column of the table. The background electric field intensity can then be calibrated according to the polarizability (shown in Table 1), which is column 5 of Table 2. Therefore, the error of the background electric field intensity measurement is caused by the statistical error of the AREF.

Optics EXPRESS

Table 2. As the principal quantum numbers are equal to 71, 75, 80, and 85, the corresponding actual resonant excitation frequency, the theoretical transition frequency (from ARC [34]), the Stark shift and the values of measured E_{bg} intensity.

Principal quantum number (n)	Actual Resonant excitation frequency (THz)	Theoretical transition frequency (THz)	Stark shift (MHz)	Measured E_{bg} intensity (mV/cm)
71	$940.814519 \pm 2.9 \times 10^{-6}$	940.814879	-359.6 ± 2.9	215.9 ± 1.6
75	$940.893047 \pm 1.5 \times 10^{-6}$	940.893609	-562.1 ± 1.5	220.9 ± 0.6
80	$940.974235 \pm 1.8 \times 10^{-6}$	940.975179	-944.2 ± 1.8	226.1 ± 0.7
85	$941.040902 \pm 1.9 \times 10^{-6}$	941.042189	-1287.2 ± 1.9	211.1 ± 0.5

As shown in Fig. 7, We plot the data in the last column of Table 2. Due to the large time span of our measurement process, there is certain fluctuations in the background electric field intensity. We find the average value of 218.9 mV/cm, which is marked with a solid red line; The difference between the maximum and minimum values of the measured value is marked as an error and is marked with a red dotted line. So, we calibrate the background electric field intensity in the vicinity of the cold cloud in MOT to 218.9 ± 7.5 mV/cm based on the results of multiple measurements.

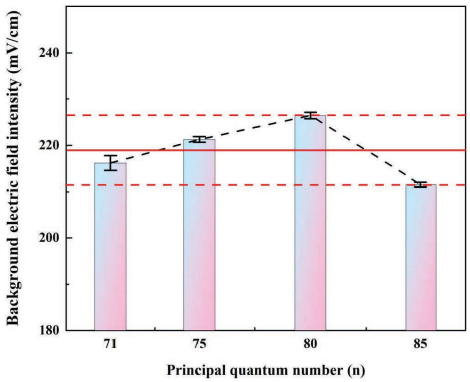

Fig. 7. Based on the DC Stark effect, we calibrated the intensity of the background electric field near the cloud of cold atoms as 218.9 ± 7.5 mV/cm by multi-measurement measurements. Error bars include contributions from statistical noise and systematic uncertainties in the measurement process.

As a DC field electrometer, we need to analyze the minimum measurable value and sensitivity.

To characterize the minimum measurable value, we selected two sets of TLFS data ($71P_{3/2}$ $m_J = \pm 3/2$), which differ by only 3 MHz in the AREF in Fig. 8(a). As shown in Fig. 8(b), both the spectra (green circle and purple star) can be clearly distinguished. The TLFS is fitted using the Lorentzian profile, and the center frequencies of the two sets of spectra are -165.3 ± 0.4 MHz and -162.9 ± 0.5 MHz, the coefficient of determination (COD) is 0.95 and 0.94, respectively. Therefore, the minimum resolving frequency of our system is 0.9 MHz, which accords to the polarizability of the $71P_{3/2}$ ($m_J = \pm 3/2$) Rydberg state in Table 1, we can estimate the minimum measurable electric field intensity is ~ 10.8 mV/cm. If the principal quantum number is increased, the polarizability increases significantly. If we use Rydberg state $85P_{3/2}$ ($m_J = \pm 3/2$), the minimum frequency resolution of 0.9 MHz of our system corresponds to a the minimum measurable electric field intensity of ~ 5.5 mV/cm.

Here, we only briefly describe the calibration method for sensitivity. In subsequent experiments, we will focus on improving the measurement sensitivity of the system. The specific scheme is

Optics EXPRESS

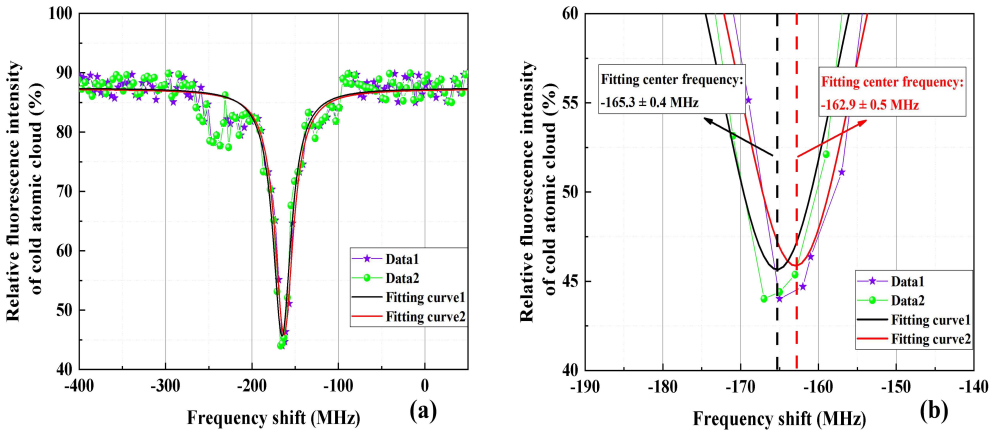

Fig. 8. Analyzing the spectral minimum resolution. (a), the two sets of TLFS (green circle and purple star) differ by about 3 MHz at center frequency and are fitted using the Lorentz function; (b) shows a magnified view of the (a), and the center frequencies of the two sets of spectra are -165.3 ± 0.4 MHz and -162.9 ± 0.5 MHz, the COD is 0.95 and 0.94, respectively. For the $71P_{3/2}$ ($m_J = \pm 3/2$) Rydberg state, we can estimate the minimum measurable electric field intensity is ~ 10.8 mV/cm. Error bars represent the confidence intervals derived from the Lorentzian fits to the experimental data. These intervals include contributions from statistical noise and systematic uncertainties in the measurement process.

as follows, by scanning the laser frequency, a photodetector is used to collect the fluorescence intensity of cold atoms, and the spectrum is measured thousands of times by using a data acquisition system. The spectrum carries the information of the external electric field, and the external electric field intensity E_{bgi} (i=1~1000) corresponding to each spectrum can be calibrated by measuring the Stark frequency shift Δf_i (i=1~1000) of each spectrum, which is a set of time-domain results, the horizontal axis is the measurement time (in s), and the vertical axis is the electric field intensity to be measured (in mV/cm). We import this set of data into the MATLAB program to do Fourier transform, and then obtain the frequency domain results, the horizontal axis is the analysis frequency (in Hz), the vertical axis is the power spectral density (in $mV/cm/Hz^{1/2}$). And the frequency statistics of the results in the frequency domain are performed, and the value with the largest number of occurrences is the measurement sensitivity of the system.

In the experiment, we continued to use the above parameters. First, we place the PCB electrode plates parallel to the vacuum cell with a distance of 35 mm, and increase the voltage between the plates from −1 V to 3 V with 0.5 V steps. As shown in Fig. 9, two typical sets of TLFS ($71P_{3/2}$ $m_J = \pm 3/2$) as a function of the electric field intensity between the plates((a), θ=0; (b), θ=20°). When no voltage is applied between the electrode plates, there is only background electric field, and the DC Stark shift is ~ -357.8 MHz (a) and ~ −360.5 MHz (b). When we increase the intensity of the electric field between the electrode plates to 300 mV/cm, the frequency bias of the TLFS reaches a minimum point of −92.3 MHz and −84.1 MHz, respectively.

Compared with the case of parallel to the UHV glass cell, the compensation effect is improved, but there is still a certain residual electric field intensity. Since the UV laser is incident from the circular hole in the middle of the plate, the angle of placement of the plate will greatly limit the incidence of UV light. Therefore, the current placement angle of 20° is optimal. However, this compensation result is not best, and we will continue to optimize the experimental system in near future to increase the diameter of the hole in order to achieve better compensation results.

Our electrometer is a scalar electrometer, which can only measure the magnitude of the electric field to be measured by measuring the Stark shift of the Rydberg state under the external electric

Optics EXPRESS

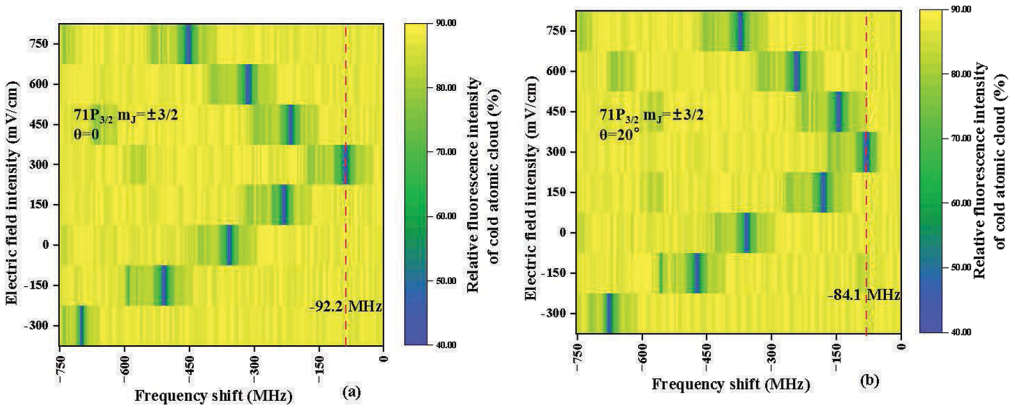

Fig. 9. Background electric field compensation by using an external electrode plate. (a) The electrode plate pair generates an electric field E parallel to the X axis; (b) The electrode plate pair generates an electric field E with an angle of 20° relative to the X axis, which changes the intensity of the applied electric field, and the Stark shift caused by the background electric field is compensated.

field. It is highly likely that the magnitude of the electric field to be measured is greater than the magnitude of the background electric field. The extra part of this is speculated to be due to a variety of ionization mechanisms that generate cold plasma near cold atoms, which in turn produces a local electric field of a certain intensity. Therefore, the measured electric field strength and the compensated electric field strength contain two parts, the background electric field in the environment and the local electric field.

The current method of using CCD cameras to capture cold atomic fluorescence pictures and point-by-point scanning can only passively compensate background electric field and is not suitable for fast feedback and active compensation. We are already in the process of upgrading our UV laser frequency scanning system and using a photodetector to collect the fluorescence of cold atoms. This scheme allows for fast scanning, acquisition, calculation of Stark shifts, estimation of background electric field strength, generation of feedback signals, and active compensation.

6. Conclusion

We use a 319-nm UV laser system to achieve single-step Rydberg excitation of cold Cs atoms confined in a MOT. The non-destructive detection of Rydberg state is realized by TLFS. By measuring the difference between the actual excitation frequencies and the theoretical values of several Rydberg states, the background electric field intensity in the vicinity of the cold cloud is got to be 218.9 ± 7.5 mV/cm. Then, we use a pair of electrode plates and change its placement angle to partially compensate the background electric field. We measured the Stark shift induced by the residual background electric field to be -84.1 MHz. This provides us with the technology and ideas for establishing a relatively pure electric field environment, and lays a foundation for further experimental research related to Rydberg atoms using UV lasers.

While the background fluctuations currently limit the practical precision, the demonstrated the minimum detectable electric field intensity indicates that our scheme could achieve highly accurate electric field measurements, particularly for weak DC electric fields. So, we will upgrade the system, improve the protocol, shorten the experimental time, and reduce the effect of ionization on the atoms, so that the background electric field intensity can be measured more accurately. In addition, we will switch to a more accurate motor to achieve precise control of the angle of the electrode plate, so as to achieve better background electric field compensation for

Optics EXPRESS

precise control of Rydberg excitation laser Rabi frequency and interactions between Rydberg atoms.

Funding. National Key Research and Development Program of China (2021YFA1402002); National Natural Science Foundation of China (12474483); Fundamental Research Program of Shanxi Province (202403021211013).

Disclosures. The authors declare no conflicts of interest.

Data availability. Data underlying the results presented in this paper may be available from the corresponding author upon reasonable request.

References

1. T. F. Gallagher, *Rydberg atoms*, (Cambridge University Press, 2005).
2. A. Browaeys and T. Lahaye, "Many-body physics with individually controlled Rydberg atoms," Nat. Phys. **16**(2), 132–142 (2020).
3. C. S. Adams, J. D. Pritchard, and J. P. Shaffer, "Rydberg atom quantum technologies," J. Phys. B: At., Mol. Opt. Phys. **53**(1), 012002 (2019).
4. M. Saffman, T. G. Walker, and K. Mølmer, "Quantum information with Rydberg atoms," Rev. Mod. Phys. **82**(3), 2313–2363 (2010).
5. M. Moreno-Cardoner, D. Goncalves, and D. E. Chang, "Quantum nonlinear optics based on two-dimensional Rydberg atom arrays," Phys. Rev. Lett. **127**(26), 263602 (2021).
6. M. Ferreira-Cao, V. Gavryusev, T. Franz, *et al.*, "Depletion imaging of Rydberg atoms in cold atomic gases," J. Phys. B: At., Mol. Opt. Phys. **53**(8), 084004 (2020).
7. C. Gross, T. Vogt, and W. H. Li, "Ion imaging via long-range interaction with Rydberg atoms," Phys. Rev. Lett. **124**(5), 053401 (2020).
8. J. A. Sedlacek, A. Schwettmann, H. Kübler, *et al.*, "Atom-based vector microwave electrometry using rubidium Rydberg atoms in a vapor cell," Phys. Rev. Lett. **111**(6), 063001 (2013).
9. D. A. Anderson, S. A. Miller, G. Raithel, *et al.*, "Optical measurements of strong microwave fields with Rydberg atoms in a vapor cell," Phys. Rev. Appl. **5**(3), 034003 (2016).
10. C. L. Holloway, J. A. Gordon, S. Jefferts, *et al.*, "Broadband Rydberg atom-based electric-field probe for SI-traceable, self-calibrated measurements," IEEE Trans. Antennas Propag. **62**(12), 6169–6182 (2014).
11. A. M. Hankin, Y.-Y. Jau, L. P. Parazzoli, *et al.*, "Two-atom Rydberg blockade using direct 6 S to n P excitation," Phys. Rev. A **89**(3), 033416 (2014).
12. A. Arias, G. Lochead, T. M. Wintermantel, *et al.*, "Realization of a Rydberg-dressed ramsey interferometer and electrometer," Phys. Rev. Lett. **122**(5), 053601 (2019).
13. M. Y. Jing, Y. Hu, J. Ma, *et al.*, "Atomic superheterodyne receiver based on microwave-dressed Rydberg spectroscopy," Nat. Phys. **16**(9), 911–915 (2020).
14. A. Osterwalder and F. Merkt, "Using high Rydberg states as electric field sensors," Phys. Rev. Lett. **82**(9), 1831–1834 (1999).
15. L. A. Jones, J. D. Carter, and J. D. D. Martin, "Rydberg atoms with a reduced sensitivity to dc and low-frequency electric fields," Phys. Rev. A **87**(2), 023423 (2013).
16. A. Schramm, J. M. Weber, J. Kreil, *et al.*, "Laser photoelectron attachment to molecules in a skimmed supersonic beam: Diagnostics of weak electric fields and attachment cross sections down to 20 μev," Phys. Rev. Lett. **81**(4), 778–781 (1998).
17. J. D. Carter, O. Cherry, and J. D. D. Martin, "Electric-field sensing near the surface microstructure of an atom chip using cold Rydberg atoms," Phys. Rev. A **86**(5), 053401 (2012).
18. J. M. Zhao, H. Zhang, Z. G. Feng, *et al.*, "Measurement of polarizability of cesium nD state in magneto-optical trap," J. Phys. Soc. Jpn. **80**(3), 034303 (2011).
19. J. D. Bai, S. Liu, J. Y. Wang, *et al.*, "Single-photon Rydberg excitation and trap-loss spectroscopy of cold cesium atoms in a magneto-optical trap by using of a 319-nm ultraviolet laser system," IEEE J. Sel. Top. Quantum Electron. **26**(3), 1–6 (2020).
20. C. Halter, A. Miethke, C. Sillus, *et al.*, "Trap-loss spectroscopy of Rydberg states in ytterbium," J. Phys. B: At. Mol. Opt. Phys. **56**(5), 055001 (2023).
21. Y. F. Cao, W. G. Yang, H. Zhang, *et al.*, "Dephasing effect of Rydberg states on trap loss spectroscopy of cold atoms," J. Phys. B: At. Mol. Opt. Phys. **39**(8), 2032–2036 (2022).
22. X. Wang, X. K. Hou, F. F. Lu, *et al.*, "Autler–townes splitting in the trap-loss fluorescence spectroscopy due to single-step direct Rydberg excitation of cesium cold atomic ensemble," AIP Adv. **13**(3), 035126 (2023).
23. J. Hostetter, J. D. Pritchard, J. E. Lawler, *et al.*, "Measurement of holmium Rydberg series through magneto-optical trap depletion spectroscopy," Phys. Rev. A **91**(1), 012507 (2015).
24. F. Karlewski, M. Mack, J. Grimmel, *et al.*, "State-selective all-optical detection of Rydberg atoms," Phys. Rev. A **91**(4), 043422 (2015).
25. W. C. Xu, A. V. Venkatramani, S. H. Cantú, *et al.*, "Fast preparation and detection of a Rydberg qubit using atomic ensembles," Phys. Rev. Lett. **127**(5), 050501 (2021).

Optics EXPRESS

26. A. D. Bounds, N. C. Jackson, R. K. Hanley, *et al.*, "Rydberg-dressed magneto-optical trap," Phys. Rev. Lett. **120**(18), 183401 (2018).
27. D. Tong, S. M. Farooqi, J. Stanojevic, *et al.*, "Local blockade of Rydberg excitation in an ultracold gas," Phys. Rev. Lett. **93**(6), 063001 (2004).
28. P. Thoumany, T. Hänsch, G. Stania, *et al.*, "Optical spectroscopy of rubidium Rydberg atoms with a 297 nm frequency-doubled dye laser," Opt. Lett. **34**(11), 1621–1623 (2009).
29. A. C. Wilson, C. Ospelkaus, A. P. VanDevender, *et al.*, "A 750-mW, continuous-wave, solid-state laser source at 313 nm for cooling and manipulating trapped $^9Be^+$ ions," Appl. Phys. B **105**(4), 741–748 (2011).
30. J. Y. Wang, J. D. Bai, J. He, *et al.*, "Development and characterization of a 2.2 W narrow-linewidth 318.6 nm ultraviolet laser," J. Opt. Soc. Am. B **33**(10), 2020–2025 (2016).
31. J. M. Wang, J. D. Bai, J. Y. Wang, *et al.*, "Realization of a watt-level 319-nm single-frequency cw ultraviolet laser and its application in single-photon Rydberg excitation of cesium atoms [invited]," Chin. Opt. **12**(4), 701–718 (2019).
32. Y.-Y. Jau, A. M. Hankin, T. Keating, *et al.*, "Entangling atomic spins with a Rydberg-dressed spin-flip blockade," Nat. Phys. **12**(1), 71–74 (2016).
33. A. Khadjavi, A. Lurio, and W. Happer, "Stark effect in the excited states of Rb, Cs, Cd, and Hg," Phys. Rev. **167**(1), 128–135 (1968).
34. N. Šibalić, J. D. Pritchard, C. S. Adams, *et al.*, "ARC: An open-source library for calculating properties of alkali Rydberg atoms," Comput. Phys. Commun. **220**, 319–331 (2017).
35. A. Kramida, Yu. Ralchenko, and J. Reader, and NIST ASD Team (2024) "NIST Atomic Spectra Database (version 5.12),," Available: https://physics.nist.gov/asd [Nov 12, 2024].
36. M. P. Robinson, B. L. Tolra, M. W. Noel, *et al.*, "Spontaneous evolution of Rydberg atoms into an ultracold plasma," Phys. Rev. Lett. **85**(21), 4466–4469 (2000).